

Review

## Dendrite Growth Kinetics in Undercooled Melts of Intermetallic Compounds

Dieter M. Herlach

Institut für Materialphysik im Weltraum, Deutsches Zentrum für Luft- und Raumfahrt, DLR, Köln 51147, Germany; E-Mail: dieter.herlach@dlr.de; Tel.: +49-2203-6012332; Fax: +49-2203-61768

Academic Editor: Duc Nguyen-Manh

Received: 2 June 2015 / Accepted: 27 August 2015 / Published: 7 September 2015

---

**Abstract:** Solidification needs an undercooling to drive the solidification front. If large undercoolings are achieved, metastable solid materials are solidified from the undercooled melt. Containerless processing provides the conditions to achieve large undercoolings since heterogeneous nucleation on container walls is completely avoided. In the present contribution both electromagnetic and electrostatic levitation are applied. The velocity of rapidly advancing dendrites is measured as a function of undercooling by a High-Speed-Camera. The dendrite growth dynamics is investigated in undercooled melts of intermetallic compounds. The Al<sub>50</sub>Ni<sub>50</sub> alloy is studied with respect to disorder trapping that leads to a disordered superlattice structure if the melt is undercooled beyond a critical undercooling. Disorder trapping is evidenced by *in situ* energy dispersive diffraction using synchrotron radiation of high intensity to record full diffraction pattern on levitated samples within a short time interval. Experiments on Ni<sub>2</sub>B using different processing techniques of varying the level of convection reveal convection-induced faceting of rapidly growing dendrites. Eventually, the growth velocity is measured in an undercooled melt of glass forming Cu<sub>50</sub>Zr<sub>50</sub> alloy. A maximum in the growth velocity–undercooling relation is proved. This is understood by the fact that the temperature dependent diffusion coefficient counteracts the thermodynamic driving force for rapid growth if the temperature of the undercooled melt is approaching the temperature regime above the glass transition temperature. The analysis of this result allows for determining the activation energy of atomic attachment kinetics at the solid–liquid interface that is comparable to the activation energy of atomic diffusion as determined by independent measurements of the atomic diffusion in undercooled Cu<sub>50</sub>Zr<sub>50</sub> alloy melt.

**Keywords:** containerless processing; undercooling of melts; intermetallics; metastable solids

---

## 1. Introduction

Metallic materials are prepared from the liquid state as their parent phase. To date, efforts are directed towards virtual material design with computer-assisted modeling. Computational materials science from the liquid state requires detailed knowledge of the physical mechanisms involved in the solidification process. In particular, these are crystal nucleation and crystal growth. Both of these processes are driven by an undercooling of the liquid below its equilibrium melting temperature to develop conditions where a driving force for the formation of supercritical nuclei and the advancement of a solidification front is created. This gives access to non-equilibrium solidification pathways, which can form metastable solids, which may differ in their physical and chemical properties from their stable counterparts. Detailed modeling of solidification, far away from thermodynamic equilibrium, requires that the solidification process has to be investigated in every detail.

In order to achieve the state of an undercooled melt, it is advantageous to remove heterogeneous nucleation sites, which otherwise limit the undercoolability. The most efficient way to realize such conditions is containerless processing of melts [1]. In such, the most dominant heterogeneous nucleation process, involving interaction with container walls, is completely avoided. Electromagnetic [2] and electrostatic levitation techniques [3,4] have been developed for containerless undercooling and solidification of molten metals and alloys. A freely suspended drop gives the extra benefit to directly observe the solidification process by combining the levitation technique with proper diagnostic means [5,6]. Short range ordering in undercooled metallic melts as precursor of crystal nucleation has been investigated by using neutron diffraction [7] and synchrotron radiation [8] on containerless undercooled melts [9]. In particular, containerless processing under ultra high vacuum condition is favorable to achieve large undercoolings from which the interfacial energy between crystal nucleus and undercooled melt may be inferred. Rapid growth of dendrites is observed on levitation undercooled melts by using high speed video camera techniques characterized by high spatial and temporal resolution [10]. In the case of containerless processing, heat is transferred by heat radiation and additionally by heat conduction in an environmental gas if the sample is processed in an inert noble gas atmosphere (e.g., in electromagnetic levitation). If the sample is largely undercooled prior to solidification, the initial crystallization process is very rapid. As a consequence the undercooled melt serves as a heat sink. This leads to a temperature rise during the initial crystallization of the sample known as recalescence.

By analyzing measured temperature–time profiles and measurements of the dendrite growth velocity as a function of undercooling disorder trapping is investigated on intermetallic compounds. Dendrite growth is controlled by heat and mass redistribution. Thus, any transport process stimulated externally by natural convection and/or forced convection due to stirring effects of alternating electromagnetic fields and/or natural convection may cause serious influence on the solidification process. To understand this effect and to develop a quantitative description of crystallization in the presence of forced convection, comparative experiments on Earth and in reduced gravity are of great help. Under the special conditions of reduced gravity, for instance in Space, the forces needed to compensate disturbing

accelerations are about three orders of magnitude smaller than the forces needed to compensate the gravitational force for levitation experiments on Earth. In a cooperative effort by the European Space Agency (ESA) and the German Aerospace Center—Space Management (DLR) a facility for Electro-Magnetic Levitation (EML) has been developed and was accommodated in the European module *Columbus* of the International Space Station (ISS) in August 2014. International research teams prepared experiments using the EML multiuser facility for investigations on undercooled metallic melts in Space [11].

The present article aims to give an overview of the present state of investigations of dendrite growth in undercooled melts of intermetallic compounds.

## 2. Experimental Details

Samples were prepared from alloy constituents all of purity of 4N5. The weight components are pre-melted in an arc furnace under high purity argon gas (6N). The samples were placed and processed in the ultra-high-vacuum chambers of electromagnetic [2] and/or electrostatic levitator [4]. The temperature is measured by pyrometers with an absolute accuracy of  $\pm 5$  K. Samples in diameter of 7 mm are processed by electromagnetic levitation. The application of electromagnetic levitation is limited since levitation force and inductive heating is coupled. In order to cool the liquid sample forced convection by helium gas is used. In the electrostatic levitator samples in diameter of 2–3 mm are processed under ultrahigh vacuum conditions ( $\approx 10^{-8}$  mbar). Levitation and heating is decoupled in contrast to the electromagnetic levitator. A high-speed video camera (Photron VKT, Video Kommunikation GmbH, Pfullingen, Germany) was applied (frame rate up to 50,000 pictures per second) to record the rapid advancement of the intersection line of the solidification front and the sample surface. A method has been developed to infer the velocity of the dendrites propagating within the bulk of the melt by projection of the interface of the solidification front and the sample surface into the interior of the drop shaped sample [12]. In this way, rapid dendrite growth velocity is measured as a function of undercooling. The measurements of dendrite growth in undercooled melts of  $\text{Al}_{50}\text{Ni}_{50}$  and  $\text{Ni}_2\text{B}$  alloys in reduced gravity were conducted using the TEMPUS facility for electromagnetic levitation in space [13] during parabolic flight campaigns.

## 3. Results and Discussions

### 3.1. Dendrite Growth Theory

Crystal growth in undercooled melts leads to heating up the solid–liquid interface due to the release of the heat of crystallization. As a consequence, a negative temperature gradient will be established in front of the interface since the undercooled melt acts as a heat sink. This will destabilize the initially planar interface. Due to limited solubility of the solute in the solid phase of alloys, compared to the liquid phase, solute will pile up in front of the interface. The resulting concentration gradient will reinforce, in addition to the negative temperature gradient, the instability of the solidification front. Eventually, the morphological destabilization of an initially planar interface will lead to dendrite growth [14]. Dendrites consist of the main stem and side-branches, which grow into the melt.

An extended model of sharp interface theory is applied to describe the growth dynamics of dendrites as a function of undercooling [15,16]. Accordingly, the total undercooling measured in the experiment is expressed as the sum of various individual contributions:

$$\Delta T = \Delta T_t + \Delta T_r + \Delta T_n + \Delta T_k + \Delta T_c \quad (1)$$

where  $\Delta T_t$  is the thermal undercooling;  $\Delta T_r$  is the curvature undercooling;  $\Delta T_n$  is the undercooling due to the shift of the equilibrium slope of the liquidus  $m_E$  to its velocity dependent value  $m_V$ ;  $\Delta T_k$  is the kinetic undercooling; and  $\Delta T_c$  is the constitutional undercooling. The thermal undercooling  $\Delta T_t = T_i - T_\infty$  with  $T_i$  the temperature at the tip of the dendrite and  $T_\infty$  the temperature of the undercooled melt far from the interface is expressed by:

$$\Delta T_t = \Delta T_{hyp} I v(Pe_t) = \frac{\Delta H_f}{C_p^l} I v(Pe_t) \quad (2)$$

$\Delta T_{hyp}$  is the hypercooling;  $\Delta H_f$  is the heat of fusion;  $C_p^l$  is the specific heat of the liquid;  $I v(Pe_t) = Pe_t \exp(Pe_t) \cdot E_1$  is the Ivantsov function for heat diffusion with  $Pe_t = (VR)/2a$  the thermal Peclet number;  $V$  is the velocity of the tip of the dendrite;  $R$  is the radius of curvature at the tip of the dendrite; and  $a$  is the thermal diffusivity;  $E_1$  denotes the first exponential integral function. Due to the strong curvature of the dendrite tip, a reduction of the melting temperature, due to the Gibbs-Thomson effect, has to be taken into account by the curvature undercooling  $\Delta T_r = T_L - T_i$  with  $T_L$  the liquidus temperature and  $T_i$  the temperature at the tip:

$$\Delta T_r = 2\Gamma(1 - 15 \varepsilon_s \cos 4\theta)/R \quad (3)$$

where  $\Gamma = \sigma/\Delta S_f$  ( $\sigma$ : interface energy,  $\Delta S_f$  the entropy of fusion) is the capillary constant (Gibbs-Thomson parameter),  $\varepsilon_s$  is the parameter of anisotropy of the interface energy, and  $\theta$  is the angle between the normal to the interface and the direction of growth along the growth-axis.  $\Delta T_n$  takes into account the change of liquidus line, due to deviations from equilibrium at large dendrite growth velocities, and is expressed by:

$$\Delta T_n = (m_E - m_V) c_o \quad (4)$$

$m_E$  is the slope of liquidus line of the equilibrium phase diagram and  $m_V$  is the slope of the liquidus line in the kinetic phase diagram at nominal composition  $c_o$ .

The kinetic undercooling  $\Delta T_k$  is given by:

$$\Delta T_k = \frac{V}{\mu}; \quad \mu = \mu_o (1 - \varepsilon_K \cos(4\theta)) \quad (5)$$

where  $\mu$  is the kinetic growth coefficient for growth of the dendrite tip,  $\varepsilon_K$  is the parameter of anisotropy for the growth kinetics [17] and is determined by atomistic simulations [18]. The kinetic undercooling is controlled by the atomic attachment kinetics at the solid-liquid interface that can differ essentially for specific atomic bonding conditions and structural peculiarities. In non-congruently melting alloys, chemical mass transport by segregation has to be considered. The constitutional undercooling in alloys with solidification interval is given by:

$$\Delta T_c = m_V c_o ((k_V - 1) I v(Pe_c)) / [1 - (1 - k_V) I v(Pe_c)] \quad (6)$$

with  $Pe_c = (VR)/2D$  the Péclet number of mass diffusion with  $D$  the diffusion coefficient,  $Iv(Pe_c) = Pe_c \cdot \exp(Pe_c) \cdot E_1$  the Ivantsov function for mass diffusion, and  $k(V)$  is the velocity dependent partition coefficient. Under the conditions of rapid solidification, for the range of growth velocity  $V < V_D$  (where  $V_D$  is the atomic diffusive speed in the bulk liquid), the liquidus slope is described by [19]:

$$m_V = \frac{m_E}{1 - k_E} \left\{ 1 - k_V + \ln\left(\frac{k_V}{k_E}\right) + (1 - k_V)^2 \frac{V}{V_D} \right\}; \quad V < V_D$$

$$m_V = \frac{m_E \ln k_E}{k_E - 1}; \quad V \geq V_D$$
(7)

with  $k_E$  the partition coefficient of the equilibrium phase diagram. The solute partitioning as a function of growth velocity is described by the non-equilibrium partition coefficient  $k_V$ , which becomes dependent on the growth velocity  $V$  for the case of rapid solidification [20]:

$$k_V = \frac{\left(1 - \frac{V^2}{V_D^2}\right) [k_E + (1 - k_e)c_o] + V/V_{Di}}{1 - \frac{V^2}{V_D^2} + V/V_{Di}}; \quad V < V_D$$

$$k_V = 1; \quad V \geq V_D;$$
(8)

with  $V_{Di}$  the interface diffusion velocity obtained by dividing the diffusion coefficient in the solid–liquid interface by the interatomic spacing. The diffusion coefficient in the interface is smaller compared with the bulk diffusion coefficient [21]. Equation (1) describes the relation of undercooling in terms of the Péclet numbers, *i.e.*, as a function of the product  $V \cdot R$ . For unique determination of the growth velocity  $V$  and tip radius  $R$  as a function of undercooling,  $\Delta T$  one needs a second equation for the tip radius  $R$ , which comes from stability analysis:

$$R = \frac{\Gamma}{\sigma_0} \left[ \frac{\Delta H_f}{C_p^l} Pe_t \xi_t(Pe_t) + \frac{2 m_V c_o (k_V - 1)}{1 - (1 - k_V) Iv(Pe_c)} Pe_c \xi_c \right]$$
(9)

$\xi_t$  and  $\xi_c$  are the stability functions depending on the thermal and the chemical Péclet number. They are given by:

$$\xi_t (Pe_t) = \frac{1}{\left(1 + a_1 \epsilon^{\frac{1}{2}} Pe_t\right)^2}$$

$$\xi_c (Pe_c) = \frac{1}{\left(1 + a_2 \epsilon^{\frac{1}{2}} Pe_c\right)^2}$$

and are defined by the stiffness  $\epsilon = 15\epsilon_c$  for a crystal with cubic symmetry and with the anisotropy  $\epsilon_c$  of the interface energy. The parameters  $\sigma_0$ ,  $a_1$ , and  $a_2$  are obtained by fitting to experimental data, or from an asymptotic analysis, as described in [22].

Since we are dealing with solidification of electromagnetically levitated drops, forced convection, induced by the strong alternating electromagnetic fields needed to levitate the drop, has to be taken into account. Accordingly, the thermal undercooling  $\Delta T_t = T_i - T_\infty$  is expressed by [23]:

$$\Delta T_t = \Delta T_{hyp} Pe_t \exp(Pe_t + Pe_t^f) \int_1^\infty q^{-1} \exp[-q Pe_t + (\ln q - q) Pe_t^f]$$
(10)

where  $Pe_T^f = U_o R / (2a)$  is the flow thermal Péclet number, with  $U_o$  the velocity of the uniformly forced flow far from the dendrite tip. We estimate the fluid flow velocity from the energy balance between the electromagnetic field, the gravitational field, and the viscous dissipation:

$$U_o = \left[ \frac{2}{\rho} (\rho g R_o) + \frac{B_o^2 \left( 1 - \exp\left(2 \frac{R_o}{\delta}\right)\right)}{8\pi} + \frac{\rho \eta^2}{2\delta^2} \right] \quad (11)$$

where  $g$  is the modulus of vector of the gravity acceleration;  $\rho$  is the mass density;  $\eta$  is the dynamic viscosity of the liquid phase;  $\delta$  is the skin depth;  $R_o$  is the radius of the sample; and  $B_o$  is the time averaged value of the magnetic field inside the levitation coil. Using typical parameters of a metallic system and regarding the boundary conditions of electromagnetic levitation experiments, typical fluid flow velocities in liquid metallic drops are determined, ranging in the order of magnitude of several tenths of centimeters per second. This is in agreement with magneto-hydrodynamic simulations and experimental observations [24].

In case of forced convection inside the melt, the stability parameter  $\sigma^*$  becomes dependent on the fluid flow velocity  $U_o$ . It is given by:

$$\sigma^* = \sigma_o \epsilon_c^{7/4} \left[ 1 + \chi(Re) \frac{U_o \Gamma}{a \Delta T_{hyp}} \right] \quad (12)$$

where  $\sigma_o$  is a constant;  $Re = U_o R / \eta$  is the Reynolds number. The function  $\chi(Re)$  can be found in [25]. For computation of the stability parameter  $\sigma^*$  we choose the results of phase-field modeling [26] with  $\sigma_o \epsilon_c^{7/4} / \sigma^* = 1.675$  for the 3D upstream fluid flow imposed on the scale of a freely growing dendrite. Thus, from the two main Equations (1) and (9), the velocity  $V$  and the tip radius  $R$  of the dendrite can be calculated as a function of the initial undercooling  $\Delta T$ .

### 3.2. Disorder Trapping in $Al_{50}Ni_{50}$

Disorder trapping occurs during rapid crystallization of undercooled melts of *intermetallics* with superlattice structure. In intermetallics, crystal growth is very sluggish at small undercoolings. The atomic attachment of atoms from the liquid to the solid needs short-range atomic diffusion, as atoms have to sort themselves out to find their proper lattice place in the superlattice structure. If undercooling increases the non-equilibrium effect of disorder trapping leads to the solidification of a metastable disordered structure.

Measurements of the dendrite growth velocity of intermetallic phases exhibit a steep rise in the growth velocity *versus* undercooling relation at a critical undercooling  $\Delta T^*$ . This change of the dendrite growth kinetics has been attributed to a transition from ordered to disordered growth of superlattice structures [27–29]. However, for  $Al_{50}Ni_{50}$  diffraction experiments on the as-solidified samples at ambient temperatures failed to prove a disordered superlattice structure [29]. This result was explained by transformations of primarily solidified disordered structures to stable ordered phases during the post-recalescence and the post-solidification period. It was shown that metastable disordered phases transform to the ordered state on a rather short time scale [30]. Transmission electron microscopy on rapidly solidified Al-Ni intermetallic alloys reveal antiphase domains, which indicate the occurrence of

disorder trapping during crystallization of drop tube processed melts [31] and rapid laser surface resolidification of Al-Ni intermetallic phases [32]. During pulsed laser melting studies on Ni<sub>3</sub>Al, a disordered fcc phase has been quenched in although an ordered L1<sub>2</sub> phase is stable up to the melting temperature, providing indirect evidence of disorder trapping during non-equilibrium solidification [33]. Nevertheless, these studies provide no direct experimental link between the occurrence of disorder trapping and the growth velocity–undercooling relationship.

Figure 1 shows the results of measurements of dendrite growth velocity as a function of undercooling for the intermetallic Al<sub>50</sub>Ni<sub>50</sub> alloy. The measured growth velocities continuously increase with undercooling. If the undercooling exceeds a value of  $\Delta T^* \approx 250$  K, a steep rise of  $V$  is observed. The intermetallic Al<sub>50</sub>Ni<sub>50</sub> alloy melts congruently. Hence, mass transport by mass redistribution and, consequently, constitutional effects can be neglected, therefore, the constitutional undercooling  $\Delta T_c \approx 0$ . Due to the large curvature radius of thermal dendrites, the curvature undercooling can be equally neglected. Therefore, the thermal undercooling and the kinetic undercooling control the dendrite growth kinetics of the intermetallic Al<sub>50</sub>Ni<sub>50</sub> compound.

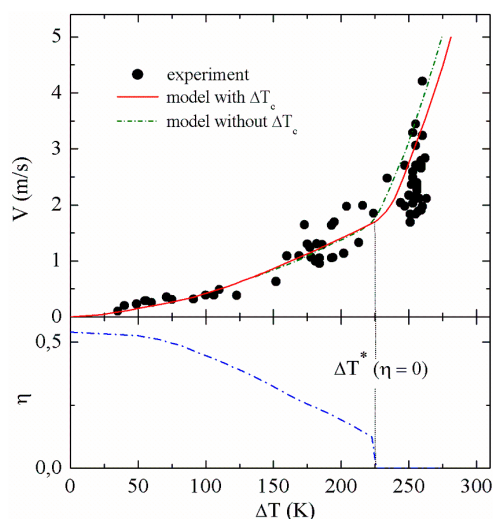


**Figure 1. (Top)** Dendrite growth velocity  $V$  as a function of undercooling  $\Delta T$  of Al<sub>50</sub>Ni<sub>50</sub> alloy measured (full circles) and computed with (solid line) and without (dashed-dotted line) constitutional undercooling  $\Delta T_c$ , assuming effects due to the shift of the congruent melting point in the kinetic phase diagram. If  $\Delta T_c = 0$  the temperature characteristics of  $V(\Delta T)$  does not change with the exception that the sharp increase of  $V$  sets in at a critical undercooling, being about 25 K smaller (dashed-dotted line); **(Bottom)** The order parameter  $\eta(V)$  is shown as a function of undercooling as inferred from the analysis of the experimental results.

The results of the measured dendrite growth velocities are analyzed within the sharp interface model. In addition to the system of equations given by this model, the non-equilibrium effect of disorder trapping has to be introduced in this concept. In order to do so, we combine the sharp interface theory with a model of disorder trapping, as developed by Boettinger and Aziz [34] that has been extended by Assadi and Greer [35]. This approach bases on the thermodynamic description in which the Gibbs free energy of the liquid,  $G_L$ , is expressed by a regular solution model and that of the solid intermetallic phase,  $G_S$ , is expressed as a function of the order parameter,  $\eta$ .  $\eta$  is defined by the difference of the fractions of atoms located in the correct and the wrong places within the superlattice of the ordered B2

structure. The link between non-equilibrium thermodynamics and crystal growth is established by three kinetic equations. One of these equations is the growth equation by Wilson and Frenkel:

$$V = V_0 \left[ 1 - \exp \left( - \frac{\Delta G_{LS}}{k_B T} \right) \right] \quad (13)$$

with  $\Delta G_{LS} = G_L - G_S$ . The solidification of the congruently melting intermetallic phase of Al<sub>50</sub>Ni<sub>50</sub> requires no long-range diffusion. Collision limited growth for the atomic attachment kinetics of atoms from the liquid to the solid is assumed so that the kinetic prefactor  $V_0$  is approximated to be the velocity of sound  $V_S$ . For sorting of the atoms on the different sublattices, however, diffusion within the solid–liquid interface is required, which is governed by the speed of interface diffusion  $V_{DI}$  and by diffusion in the bulk liquid,  $V_D$ , which are two to three orders of magnitude smaller than  $V_S$ . The balance of the mass fluxes to the different sublattices of the more or less ordered solid phase during crystal growth defines two other kinetic equations [29,36]. Apart from thermodynamic and kinetic parameters, the equation system depends on five variables. These are the temperature of the solid–liquid interface  $T_i$ , the composition of the solid,  $c_s$ , and of the liquid phase,  $c_l$ , the order parameter  $\eta$ , and the growth velocity  $V$ . For a given  $V$  and at a fixed nominal composition of the liquid,  $c_l$ , the other three variables,  $c_s$ ,  $T_i$  and  $\eta$  can be determined by numerically solving the equation system. Hence, the model provides a description for the velocity dependence of the order parameter  $\eta(V)$ . Moreover, by linking  $c_l$ ,  $c_s$ , and  $T_i$ , it allows for calculating a metastable phase diagram in which the liquidus temperature line depends on the velocity  $V$ , thus,  $T_L(V)$ . From this kinetic phase diagram, the kinetic undercooling  $\Delta T_K$  (difference between local equilibrium liquidus and velocity dependent liquidus temperature),  $k_V$  and  $m_V$  are directly inferred. More details of the computations are given in [37].

The results of the computations of dendrite growth velocity as a function of undercooling are given in the upper part of Figure 1 (solid line). It is evident that the predictions of the extended sharp interface model are in reasonable agreement with the experimental results over the entire range of undercooling accessible by application of the electromagnetic levitation technique.

At large undercoolings, the model reproduces the sharp increase of  $V$  at  $\Delta T^*$ . Small constitutional effects by the slight shift of the congruent melting point in the kinetic phase diagram are taken into account in the present calculations. If these constitutional effects are neglected, the critical undercooling at which  $V$  steeply rises is slightly shifted to lower undercoolings (*cf.* dashed-dotted line in Figure 1). The variation of the order parameter  $\eta$  with undercooling as predicted by the model of disorder trapping [27,37] is shown in the lower part of Figure 1. It continuously decreases with increasing undercooling and drops suddenly to zero at an undercooling at which disorder trapping sets in as indicated by the sharp increase of dendrite growth velocity in the upper part of Figure 1. Even for small velocities, the order parameter is considerably smaller than unity because some degree of disorder is favorable at elevated temperatures due to the entropic term in the Gibbs free energy.

These experiments give the direct relation of dendrite growth velocity and disorder trapping at large undercoolings. However, investigations of solid samples solidified at large undercoolings do not reveal a disordered B2 structure. This surprising result finds an explanation by *in situ* Energy-Dispersive X-ray Diffraction (EDXD) on levitation undercooled Al<sub>50</sub>Ni<sub>50</sub> melts using synchrotron radiation at the European Synchrotron Radiation Facility Grenoble. Figure 2 shows diffraction spectra recorded during rapid solidification of two Al<sub>50</sub>Ni<sub>50</sub> alloy undercooled less than 225 K (left) and undercooled more than 225 K. The inserts display temperature–time profiles during which X-ray diffraction spectra are

recorded: in the undercooled liquid state (A), during recalescence (B), and during post-recalescence period (C). The spectra A reflect the characteristic feature of a liquid with a halo at low diffraction angle. The spectra B give the superposition of the spectrum of the liquid with primarily crystallized phase. There is an important difference of the spectra B on the left hand and on the right hand side. While in the spectrum of the sample undercooled less than 225 K a peak appears that is ascribed to the superlattice structure of B2 ( $\beta$ ) phase this peak is missing in spectrum B of the sample undercooled more than 225 K. This gives direct evidence that the B2 phase is primarily solidifying in disordered superlattice structure in the sample undercooled more than the critical undercooling  $\Delta T^* = 225$  K as inferred from the growth velocity *versus* undercooling measurements as depicted in Figure 1.

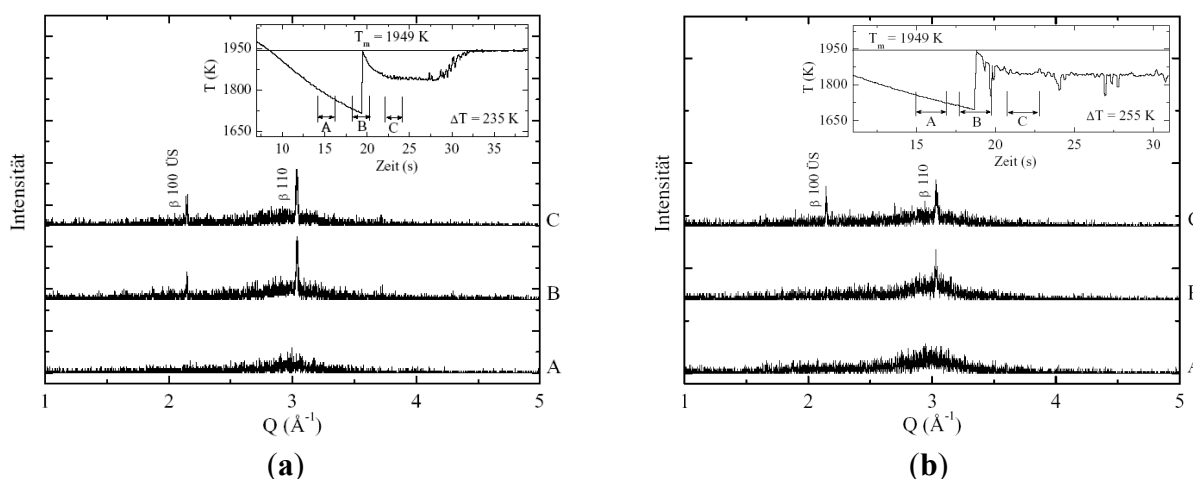


**Figure 2.** Energy Dispersive X-ray Diffraction (EDXD) spectra recorded on levitation undercooled  $\text{Al}_{50}\text{Ni}_{50}$  alloy using synchrotron radiation at the European Synchrotron Radiation Facility (ESRF) Grenoble. The inserts give the temperature time profiles with the time periods during which an EDXD spectrum is recorded, in the undercooled melt (A), during recalescence (B), and during post-recalescence period (C). The left spectra (a) are taken on a sample undercooled less than 225 K while the right spectrum (b) is recorded on a sample undercooled more than 225 K. It is obvious that the spectra B differ. While, in the B spectrum on the left hand side, the diffraction peak of the ordered B2 ( $\beta$ ) phase (denoted by  $\beta$  100  $\text{ÜS}$ ) is clearly detected it is missing in the B spectrum on the right hand side. This result gives direct evidence that disorder trapping leads to the formation of a primarily solidified disordered superlattice structure provided that the sample is undercooled more than the critical undercooling  $\Delta T^* = 225$  K that has been determined by the measurements of the dendrite growth velocity  $V$  as a function of undercooling  $\Delta T$  (*cf.* Figure 1).

However, the diffraction peak of the ordered B2 ( $\beta$ ) phase reappears in spectrum C on the right hand side of Figure 2. Obviously, the disordered B2 phase is ordering during post-recalescence period. This can be understood taking into account the small cooling rate and the short diffusion time, respectively. The cooling rate in the present experiments is small in the order of 1–10 K/s. On the other hand, ordering of a disordered superlattice structure needs only short-range diffusion and hence small diffusion time. Accordingly, this explains why the disordered B2 phase cannot be detected in the microstructure analysis of samples undercooled more than 225 K. It is concluded that the analysis of as-solidified microstructures does not tell the entire truth of primarily solidification processes.

### 3.3. Convection and Dendrite Growth

So far, experiments of dendrite growth velocities have been presented which give evidence for various effects of non-equilibrium solidification at large dendrite growth velocities. At moderate and small growth velocities, there will be an influence of convection in heat and mass transport that controls the dendrite growth kinetics. In electromagnetic levitation experiments, strong stirring of the melt by the induced eddy currents leads to forced convection. The fluid flow velocity  $U$  estimated for such experiments are ranging up to 0.6 m/s. Therefore, one expects an influence of forced convection in the dendrite growth velocity range  $V \leq U$  [24,38].

Al<sub>50</sub>Ni<sub>50</sub> was chosen for the investigations on growth kinetics under the conditions of forced convection on Earth and small convection in reduced gravity [39]. This alloy melts congruently and forms an intermetallic B2  $\beta$ -phase under equilibrium conditions. Crystallization of ordered superlattice structures requires short-range atomic diffusion at the solid–liquid interface. This leads to sluggish growth dynamics, at least at small and intermediate undercoolings ( $V$ : 0.1–0.5 m/s) [40]. These growth velocities are directly comparable to the speed of fluid flow in levitated metallic melts. Fluid flow motion inside the liquid drop changes the growth dynamics.

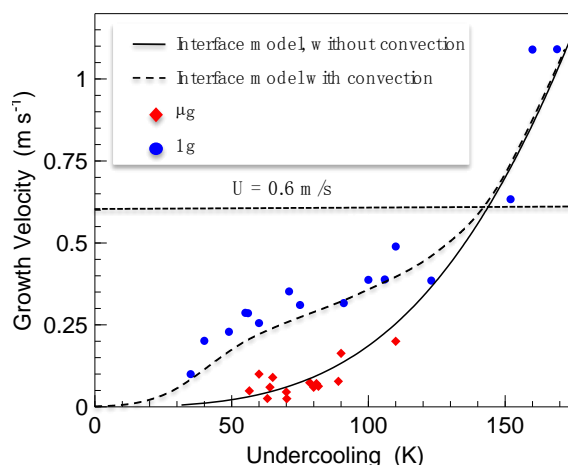


**Figure 3.** Dendrite growth velocity of B2  $\beta$ -phase of Al<sub>50</sub>Ni<sub>50</sub> alloy as a function of undercooling measured under terrestrial conditions (circles) and in reduced gravity (diamonds). The solid line represents the prediction of dendrite growth theory without convection and the dashed line with convection.  $U$  denotes the speed of fluid flow inside an electromagnetically levitated droplet as estimated by magneto-hydrodynamic simulations [24].

This effect will be reduced if the liquid drops are processed in a reduced gravity environment since convection is much less pronounced. Figure 3 shows the results of measurements of dendrite growth velocity as a function of undercooling for Al<sub>50</sub>Ni<sub>50</sub> alloy, both under terrestrial conditions (circles) and in reduced gravity (diamonds). All growth velocities measured in reduced gravity are significantly smaller than those determined under terrestrial conditions in the growth velocity range  $V < U$ . At growth velocities exceeding the fluid flow velocity  $V > U \approx 0.6$  m/s, data of dendrite growth velocity from terrestrial and from reduced gravity experiments coincide. The results of sharp interface modeling neglecting the influence of fluid flow are depicted in Figure 3 (solid line). It describes the experimental results obtained in reduced gravity. The sharp interface model is able to reproduce the experimental

results in the regime  $V < U$ , if a fluid flow velocity of  $U \approx 1.2$  m/s, is assumed for the calculations within the frame of the sharp interface theory (*cf.* dashed line in Figure 3). At growth velocities  $V > 0.6$  m/s, the computed relation of  $V = f(\Delta T)$ , without and with convection, converge to one line since, in this region, the dynamics of solidification is mainly limited by thermal diffusivity.

#### 3.4. Microstructure Development in Ni<sub>2</sub>B

Convection does not only influence the dendrite growth kinetics but also affects microstructure evolution. A particular interesting finding is observed in measurements of the dendrite growth velocity as a function of undercooling of intermetallic Ni<sub>2</sub>B alloy. This alloy system is characterized by a dimensionless entropy of fusion  $\Delta S_f/R \approx 2$  ( $\Delta S_f$ : entropy of fusion, R: gas constant). According to Jackson's rule, such a value of the reduced entropy of fusion ranges between  $\Delta S_f/R = 1$  and  $\Delta S_f/R = 3$ .  $\Delta S_f/R = 1$  is known for metallic systems of more or less isotropic bonding. These systems show a rough interface on the atomic scale and dendritic microstructures on a mesoscopic scale. On the other hand,  $\Delta S_f/R = 3$  is known for systems with strong anisotropic bonding as present in covalent systems. These systems show a smooth interface on an atomic scale and faceted microstructures on a mesoscopic scale. Similar to other intermetallic systems growth kinetics is sluggish. Therefore, one would expect that convection affects both the growth kinetics and microstructure evolution.

We have investigated the solidification of undercooled melt of Ni<sub>2</sub>B alloy under different conditions of convection. Different techniques were applied to measure the dendrite growth kinetics as a function of undercooling all of them creating various levels of convection. These are electromagnetic levitation on Earth, forced convection, electromagnetic levitation in reduced gravity, reduced forced convection, melt fluxing technique, natural convection only, melt fluxing in a strong external magnetic field, reduced natural convection, and eventually electrostatic levitation on small samples with almost no convection [41].

The Ni<sub>2</sub>B dendrite growth velocity along the (111) normal directions as a function of undercooling measured under different convective flow conditions is presented in Figure 4. The error bars result from uncertainties in the fitting procedure, e.g., from samples not being perfectly spherical and/or partially hidden by the levitation coil in EML. The growth velocities measured up to  $\Delta T_{\max} = 272$  K are well below 1 m/s and are thus comparable with or even less than the expected fluid flow velocities present in 1 g EML. The growth velocity  $V(\Delta T)$  is found to increase monotonically. As can be seen in Figure 4, for undercoolings  $40 \text{ K} < \Delta T < 150 \text{ K}$ , the growth velocity increases with the fluid flow velocity. The lowest growth velocities are obtained by ESL, followed by the melt fluxing (MF) and  $\mu\text{g}$  EML, whereas the highest values are obtained by 1 g EML. Indeed, as soon as convection may play a not negligible role in solidification kinetics, we observed the increase of dendrite growth velocity. This is in close agreement with the predicted order of the flow velocities in the various experiment techniques. In the presence of an external static magnetic field of 1.2 Tesla, the growth velocities obtained by MF are slightly shifted to lower values, which, within the limit of accuracy, overlap with the ESL values. Deviations may be due to the influence of residual flow that is not completely stabilized by the magnetic field. Interestingly, the results obtained by  $\mu\text{g}$  EML are quite close to the velocities measured under the condition of natural convection in MF.

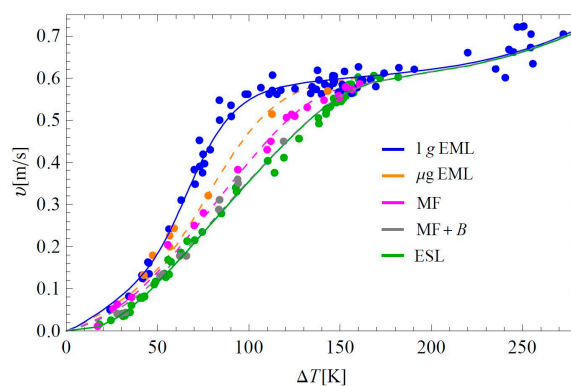


**Figure 4.** Dendrite growth velocities as a function of undercooling of Ni<sub>2</sub>B alloy for various fluid flow velocities: ESL:  $u = 0.00$  m/s, MF + B:  $u = 0.01$  m/s, MF:  $u = 0.05$  m/s,  $\mu$ g EML:  $u = 0.18$  m/s, and 1 g EML:  $u = 0.25$  m/s, respectively.

For  $\Delta T < 40$  K as well as  $\Delta T \geq 150$  K, the data coincide within the uncertainty of the measurements. This is physically reasonable since, on the one hand, the growth velocity must vanish for  $\Delta T = 0$  K and, on the other hand, the influence of convection is likely to become less pronounced in the high-velocity region. The difference in the growth velocities in the medium undercooling range is due to an apparent change in the slope of the 1 g EML  $V(\Delta T)$  data measured under the condition of forced convection. This results in a significant gap of roughly 60% at  $\Delta T \approx 100$  K between the ESL and 1 g EML data of growth velocities, which may be attributed to an enhanced heat and mass transfer due to electromagnetically induced convection.

For the further analysis, we apply the sharp interface model taking into account heat transport by convection similar to the case of the Al<sub>50</sub>Ni<sub>50</sub> alloy. However, surprisingly, this does not lead to a reproduction of the experimental results. In addition, taking into account small shifts in the concentration from the stoichiometric composition of Ni<sub>2</sub>B alloy, which may occur during the processing the samples at high temperatures due to evaporation is not satisfactory [42].

Growth in Ni<sub>2</sub>B is predominantly governed by the kinetic contribution to the total undercooling. The kinetic undercooling is controlled by atomic attachment kinetics at the solid–liquid interface. It depends on the interface morphology. In general, it can be categorized either as atomically smooth (faceted) or atomically diffuse (rough). In the first case, the solid–liquid interface is thin, in the order of one atomic layer, while, in the second case, the interface is rather diffuse over several atomic layers. According to Jackson, the atomic arrangement at the interface depends mainly on the entropy of fusion  $\Delta S_f$  [43]. If the dimensionless entropy  $\Delta S_f/R_G < 2$  ( $R_G$ : gas constant), a rough interface will be favored, while, for  $\Delta S_f/R_G > 2$ , a smooth interface will be preferentially formed [44]. Pure metals are often characterized by  $\Delta S_f \approx R_G$  and are predicted to have a rough interface. However, many intermetallic compounds show high entropy of fusion due to strong chemical bonding and, consequently, a smooth faceted interface will be formed. Faceted interfaces have inherently a low accommodation factor  $f < 1$  in contrast to  $f = 1$  for metals. This means not each atomic jump from the liquid to the solid will be successful. In such a case, the interface undercooling as given in Equation (5) can be written as [45]

$$\Delta T_k = \left(\frac{V}{\mu}\right)^n \quad (14)$$

where the kinetic exponent  $n$  is determined from experiments. The 1 g EML results can be reproduced much more accurately by setting  $n < 1$ . For pure faceted spiral growth,  $n = 0.5$  [46]. It is found that the

increase in growth velocity, as observed in 1 g EML, is only partly due to the influence of electromagnetically driven flow on the thermal and solute concentration fields in front of the solid–liquid interface but can be mainly attributed to the substantial change in growth kinetics caused by a convection induced transition from dendrites to more faceted solidification structures. The parameters used for fitting the experimental results are collected in Table 1.

**Table 1.** Best fit parameters used to calculate the Ni<sub>2</sub>B growth velocities as shown in Figure 4. The kinetic growth coefficient  $\mu$  is obtained for  $f \cdot v_s = 4.25$  m/s.

Experiment	Stability Parameter *	Fluid Flow Velocity $u$ (m/s)	Kinetic Exponent $n$
1 g EML	$5.0 \times 10^{-5}$	0.25	0.85
$\mu$ g EML	$7.0 \times 10^{-5}$	0.18	0.93
MF	$9.0 \times 10^{-5}$	0.05	0.98
MF + B	$1.0 \times 10^{-4}$	0.01	1.00
ESL	$1.0 \times 10^{-4}$	0.00	1.00

This change is supported by investigating the microstructures of samples solidified upon undercooling in ESL and EML. Figure 5a displays the microstructure of a sample solidified under the condition of no convection (ESL), while Figure 5b gives the structure of a sample solidified under the conditions of forced convection (EML) [47]. Samples processed in ESL exhibit the regular dendritic pattern. In contrast, the smooth structure of samples processed in EML shows a transition to irregular rod-shaped structures. Apparently, the internal structure resembles the well-known morphology of so-called Hopper crystals, which are rarely found for metallic materials but are often observed in non-metallic systems. The structure found in Ni<sub>2</sub>B processed in EML under the conditions of forced convection is compared to Bi and PbTe hopper crystals in Figure 6.

A hopper crystal is usually formed due to a disparity of growth rates, *i.e.*, the crystal edges are growing more rapidly than the crystal faces. This is a typical example of faceted growth on a more local level [48]. Hopper crystals have been reported for non-metallic forsterite (Mg<sub>2</sub>SiO<sub>4</sub>) [49] and PbS single crystals [50]. Faceted growth is expected in systems of high entropy of fusion  $\Delta S_f$ , as e.g., in Bi,  $\Delta S_f = 2.4R_G$ . This is larger than  $\Delta S_f = 2R_G$  as in the present case of Ni<sub>2</sub>B. Obviously, forced convection induces faceting of the solid–liquid interface in systems, which show otherwise growth of a rough solid–liquid interface of metallic systems.

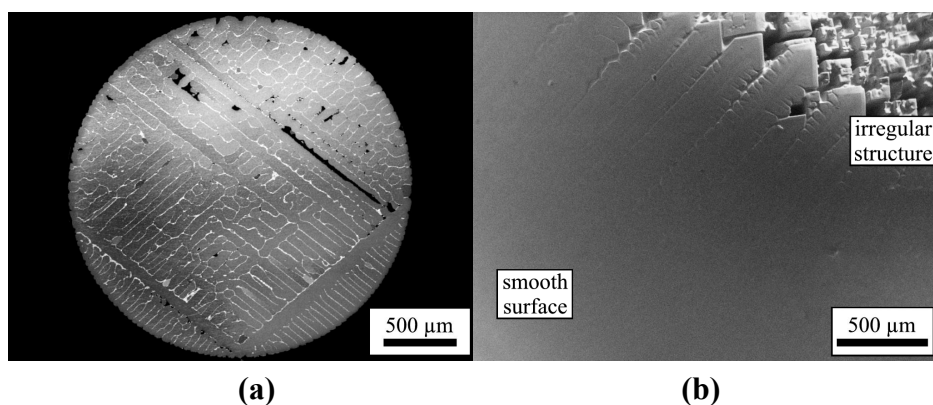


**Figure 5.** (a) Structure of a sample solidified without convection (ESL); (b) Structure of a sample solidified with forced convection (EML).

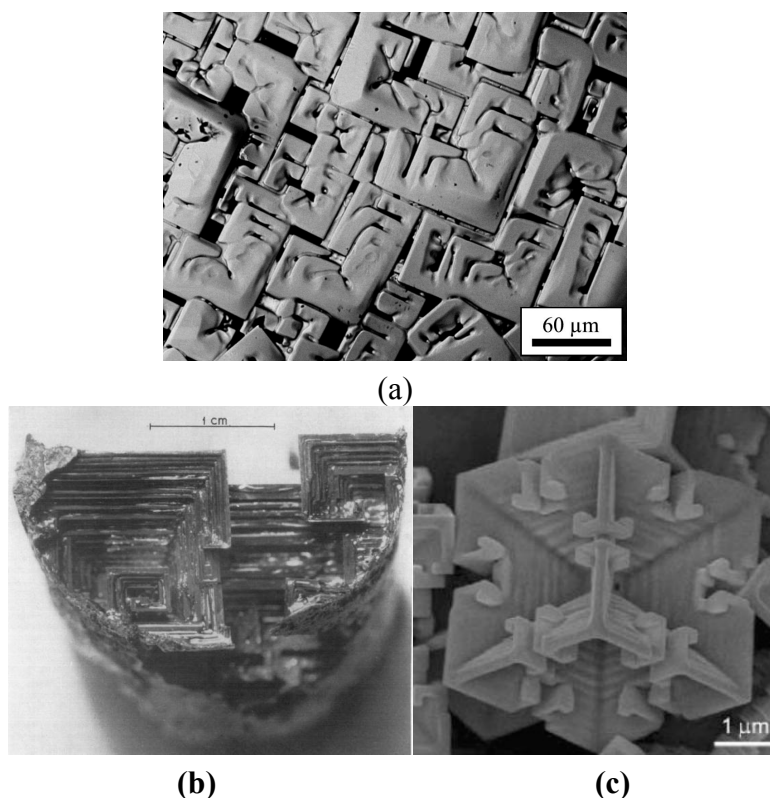


**Figure 6.** (a) The structure of the  $\text{Ni}_2\text{B}$ -rod like morphology solidified under the conditions of forced convection (EML); (b) hopper crystals found in Bi [48], and (c) PbTe [42].

### 3.5. Dendrite Growth of $\text{Cu}_{50}\text{Zr}_{50}$

So far, the majority of the measured velocity–undercooling ( $V - \Delta T$ ) relations in metallic systems show a monotonous increase of  $V$  with  $\Delta T$ . In this case, the energetics controls the growth [51]. In glass-forming systems, however, the mobility of the atomic movement rapidly decreases if  $\Delta T$  is approaching  $\Delta T_g = T_l - T_g$  with  $T_l$  the liquidus and  $T_g$  the glass transition temperature. In the temperature range at large undercoolings where the temperature of the undercooled liquid approaches the glass transition temperature  $T_g$ , the steeply decreasing diffusion coefficient eventually overcomes the acceleration of the interface by the thermodynamic driving force for crystallization. The latter one is given by the Gibbs free energy difference  $\Delta G = G_l - G_s$  with  $G_l$  and  $G_s$  the Gibbs free energy of liquid and solid, respectively. This leads to a maximum in the  $V - \Delta T$  relation. This was experimentally observed in a great variety of non-metallic glass-forming systems, such as *o*-terphenyl [52], tri- $\alpha$ -naphthylbenzene [53],  $\text{Li}_2\text{O}-2\text{SiO}_2$  [54], and  $\text{MgO}-\text{CaO}-2\text{SiO}_2$  [55]. However, so far, there is only one work that reports a maximum in the  $V-\Delta T$  relation measured for the  $\text{Cu}_{50}\text{Zr}_{50}$  glass-forming alloy [56].

The results of the measurements of  $V$  as a function of  $\Delta T$  are shown in Figure 7. The squares give the experimental data. Taking the values of the melting temperature and the glass temperature of  $\text{Cu}_{50}\text{Zr}_{50}$ , the difference between  $T_l = 1209$  K and  $T_g = 670$  K, is determined as  $\Delta T_g = 539$  K. This corresponds to a relative glass temperature  $T_g/T_l = 0.56$  [57]. Such a high value is indicative for an excellent glass forming ability [58]. A maximum in the  $V - \Delta T$  relation is experimentally observed. It indicates that at undercoolings less than the undercooling of the maximum growth velocity, dendrite growth is controlled by the thermal transport, while at undercoolings larger than the undercooling of the maximum growth velocity, dendrite growth is governed by atomic diffusion. The maximum undercooling achieved in the

experiment is approaching the temperature range above the glass temperature where the rapidly decreasing diffusion coefficient progressively influences the atomic attachment kinetics and thus the mobility of the solidification front.

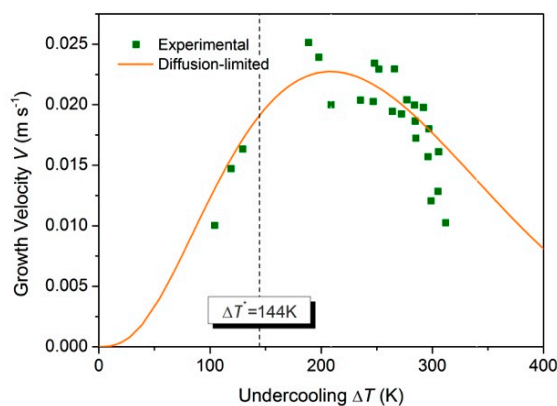


**Figure 7.** Measured growth velocity  $V$  as a function of undercooling  $\Delta T$  (squares). There is a specific undercooling: At  $\Delta T^* = 144$  K the thermal undercooling  $\Delta T_t$  equals to the kinetic undercooling  $\Delta T_k$ , Solid line gives the prediction of dendrite growth theory assuming diffusion-limited growth and taking into account a temperature dependent diffusion coefficient (see the text).

The experimental results are analyzed within the sharp interface model, as described in Section 3.1. Taking into account the dependence of the diffusion coefficient on the temperature extends this model. The  $\text{Cu}_{50}\text{Zr}_{50}$  is an intermetallic compound, which melts congruently. Therefore, constitutional contributions to the undercooling can be excluded similar as in the case of  $\text{Al}_{50}\text{Ni}_{50}$  compound discussed in a previous chapter. In addition, the curvature undercooling is neglected because this contribution is small for thermal dendrites with their large curvature radius at the tip. Therefore, the total undercooling is approximated by  $\Delta T \approx \Delta T_T + \Delta T_K$ . The kinetic undercooling  $\Delta T_K$  is controlled by the atomic attachment kinetics at the solid–liquid interface. In the case of an intermetallic compound, such as  $\text{Cu}_{50}\text{Zr}_{50}$ , and even more because of the good glass-forming ability of this alloy, the atomic attachment kinetics will be diffusion controlled. In this case the prefactor  $V_0$  in Equation (13) shall correspond to the atomic diffusive speed,  $V_d$ . Equation (13) is then rewritten as

$$V = V_D \left( 1 - \exp\left(-\frac{\Delta G_{LS}}{k_B T}\right) \right) \quad (15)$$

with

$$V_D = CD_l = CD_0 \exp\left(-\frac{Q_D}{R_g T_l}\right) \quad (16)$$

where  $D_l(T)$  is the temperature dependent diffusion coefficient in the liquid and  $Q_d$  is the activation energy for diffusion. This is the case when ordering in the liquid [59,60] is necessary for crystallization [61]. The activation energy of crystallization in a number of metals and alloys is the same as for diffusion [62]. Obviously, the diffusion-limited crystallization mode prevails even in pure metals at large undercoolings, e.g., it seems thermally-limited for Ag at low  $\Delta T$  [63] but is actually diffusion-limited on the whole for  $\Delta T$  up to  $\Delta T_g$  [64]. According to Aziz and Boettinger [27], the

pre-factor  $C$  in Equation (15) is defined as  $C = f/\lambda$  with  $\lambda$  the interatomic spacing and  $f$  a geometrical factor of order unity. If  $\lambda = 1.98 \text{ \AA}$  is given as the average lattice spacing normal to (100) and (110) surfaces in the MD simulation [65], the inter-diffusion coefficient  $D_i = V_0\lambda/f$  can be determined.

For further analysis, each experimental point is fitted with the dendrite growth model to obtain the upper limit of the growth velocity  $V_0$  at each measured undercooling  $\Delta T$ .  $V_0$  is then plotted as a function of  $1000/T_i$  in a semi-logarithmic diagram, as shown in Figure 8. It is interesting to see that the evolution of  $V_0$  with  $T_i$  follows the Arrhenius law except for the last three experimental points at high  $\Delta T$ . This means that crystallization of  $\text{Cu}_{50}\text{Zr}_{50}$  melt is thermally activated with a prefactor  $CD_0 = 1425.8 \text{ m/s}$  and an activation energy  $Q_D = 79759 \text{ J/mol} = 0.827 \text{ eV}$ . Based upon these results, the dendrite growth velocity  $V$  is calculated as a function of the total undercooling  $\Delta T$ . The results of these computations are presented as the solid line in Figure 7. One can see the experimental results of the dendrite growth velocity are well reproduced. A maximum  $V = 0.023 \text{ m/s}$  is found at  $\Delta T = 209 \text{ K}$ , which is quite close to the experimental measurement of a maximum  $V = 0.025 \text{ m/s}$  at  $\Delta T = 200 \text{ K}$ . It is interesting to note that using the temperature dependent viscosity does not lead to a matching of the experiments and the modeling [56], in contrast to the present work where the temperature dependent diffusion coefficient is used to take into account the mobility of the solid–liquid interface. This may be understood by the fact that the Einstein–Stokes relation does not hold for Zr-based glass forming alloys [66].

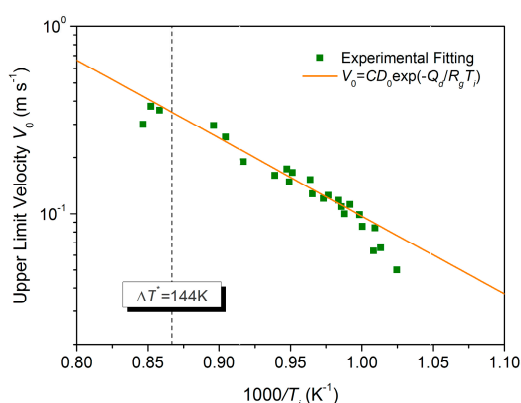


**Figure 8.** Arrhenius plot of the upper limit of growth velocity  $V_0$  as a function of 1000 times the reciprocal interface temperature  $1000/T_i$ : experimental data (squares); results of the computations (solid line).

As to a similar undercooled glass-forming  $\text{Ni}_{50}\text{Zr}_{50}$  alloy from which a stoichiometric compound  $\text{NiZr}$  is crystallized, the self-diffusion coefficient of Ni  $D_{\text{Ni}}$  was measured [67]. The activation energy for the atomic diffusion is determined as  $Q_d = 0.73 \pm 0.03 \text{ eV}$ , which is very close to the value inferred from the slope of the computed line in Figure 7,  $Q_d = 0.827 \text{ eV}$ . If  $D_{\text{Ni}}$  is extended to low temperatures, there are no large differences between  $D_{\text{Ni}}$  and the current result inferred from the dendrite growth measurements in undercooled  $\text{Cu}_{50}\text{Zr}_{50}$  alloy. The temperature dependent self-diffusion coefficients of Cu,  $D_{\text{Cu}}$  and, Zr,  $D_{\text{Zr}}$  were investigated by MD simulations for  $\text{Cu}_{50}\text{Zr}_{50}$  [67]. The activation energies, as determined from these results, lead to the activation energies of the atomic self-diffusion for Cu and Zr,  $Q_{\text{Cu}} = 0.42 \text{ eV}$  and  $Q_{\text{Zr}} = 0.44 \text{ eV}$  [65]. Despite potential significant uncertainties due to the difference in the interatomic potentials, the current diffusion coefficient and its activity energy are within the uncertainty of MD simulation results. Thus, it is quite reasonable to conclude that crystallization of undercooled  $\text{Cu}_{50}\text{Zr}_{50}$

alloy is diffusion-limited through the undercooling range where the interface undercooling is dominant. The deviations at high  $\Delta T$  (Figures 7 and 8) are attributed to two effects. First, the anisotropy effect of kinetic coefficient, which is quite important for selecting the operating state of dendrite [68], especially at high  $\Delta T$ , is not considered in the solvability theory. Second, the diffusion changes from the thermally activated single atom to the collective atomic mechanism when  $T \rightarrow T_g$  and the Arrhenius law cannot hold at very high  $\Delta T$  [69,70].

#### 4. Conclusions

Containerless processing by electromagnetic and electrostatic levitation has been applied to investigate topological order in undercooled metallic melts. Very large undercoolings were achieved. Dendrite growth kinetics was studied in detail at very large undercoolings. Non-equilibrium effects have been detected by measurements of the dendrite growth velocity as a function of undercooling. Disorder trapping was studied by undercooling experiments on the intermetallic compound  $\text{Al}_{50}\text{Ni}_{50}$ . By measurements of the dendrite growth velocity at very large undercoolings, a transition from ordered to disordered growth of the B2  $\beta$ -phase was identified. By taking into account a velocity dependent order parameter, dendrite growth theory was extended such that it describes quantitatively the dendrite growth velocity over the entire undercooling range accessible by containerless processing and reproducing the transition from ordered to disordered growth. This leads to the solidification of a metastable disordered superlattice structure of the intermetallic compound.

Comparative experiments on Earth, and in reduced gravity, of measurements of dendrite growth in undercooled  $\text{Al}_{50}\text{Ni}_{50}$  clearly reveal the importance of forced convection on growth dynamics, which has to be taken into account to predict growth dynamics in undercooled melts. Investigations of both dendrite growth kinetics and microstructure evolution on the intermetallic compound  $\text{Ni}_2\text{B}$  under different conditions of convection give evidence that forced convection leads to a transition from dendrite-like growth to faceted growth.

Finally, a glass forming binary metallic alloy,  $\text{Cu}_{50}\text{Zr}_{50}$ , was investigated with respect to its dendritic growth dynamics. For the first time, a maximum in the dendrite growth velocity–undercooling relation was observed for a metallic alloy, which is a common feature for non-metallic glass forming systems. The analysis of these experiments reveals diffusion controlled growth in particular in the regime of temperatures between the maximum growth velocity to the glass transition temperature.

All of these investigations prove containerless processing to be a powerful experimental tool to investigate phenomena of solidification, which are far away from equilibrium. They lead to various solid metastable materials. Hence, undercooling is an effective parameter to control phase selection during solidification.

#### Acknowledgments

The author thanks Peter Galenko, Jan Gegner, Dirk Holland-Moritz, Matthias Kolbe, Thomas Volkmann, and Hafeng Wang for excellent cooperation and fruitful discussions. Financial support by Deutsche Forschungsgemeinschaft within contracts HE1601/18, HE1601/21, HE1601/25, and HE1601/26, DLR Space Agency within contract 50WM1140, and the European Space Agency within contract 15236/02/NL/SH is gratefully acknowledged.

## Conflicts of Interest

The authors declare no conflict of interest.

## References

1. Herlach, D.M.; Cochrane, R.F.; Egry, I.; Fecht, H.-J.; Greer, A.L. Containerless processing in the study of metallic melts and their solidification. *Inter. Mater. Rev.* **1993**, *6*, 273–347.
2. Herlach, D.M. Containerless undercooling and solidification of pure metals. *Annu. Rev. Mater. Sci.* **1991**, *21*, 23–92.
3. Rhim, W.-K.; Chung, S.K.; Barber, D.; Man, K.F.; Gutt, G.; Rulison, A.J.; Spjut, R.E. An electrostatic levitator for high-temperature containerless processing in 1-g. *Rev. Sci. Instrum.* **1993**, *64*, 2961–2970.
4. Meister, T.; Werner, H.; Lohoefer, G.; Herlach, D.M.; Unbehauen, H. Gain-scheduled control of an electrostatic levitator. *Eng. Pract.* **2003**, *11*, 117–128.
5. Notthoff, C.; Franz, H.; Hanfland, M.; Herlach, D.M.; Holland-Moritz, D.; Petry, W. Energy-dispersive X-ray diffraction combined with electromagnetic levitation to study phase-selection in undercooled melts. *Rev. Sci. Instrum.* **2000**, *71*, 3791–3796.
6. Shuleshova, O.; Löser, W.; Holland-Moritz, D.; Herlach, D.M.; Eckert, J. Solidification and melting of high-temperature materials: *In situ* observations by synchrotron radiation. *J. Mater. Sci.* **2012**, *47*, 4497–4513.
7. Schenk, T.; Holland-Moritz, D.; Simonet, V.; Bellisent, R.; Herlach, D.M. Icosahedral short-range order in deeply undercooled metallic melts. *Phys. Rev. Lett.* **2002**, *89*, doi:10.1103/PhysRevLett.89.075507.
8. Kelton, K.F.; Lee, G.W.; Gangopadhyay, A.K.; Hyers, R.W.; Rathz, T.; Rogers, J.; Robinson, M.B.; Robinson, D.S. First X-ray scattering studies on electrostatically levitated metallic liquids: demonstrated influence of local icosahedral order on the nucleation barrier. *Phys. Rev. Lett.* **2003**, *90*, doi:10.1103/PhysRevLett.90.195504.
9. Kelton, K.F.; Greer, A.L.; Herlach, D.M.; Holland-Moritz, D. The influence of order on the nucleation barrier. *Mater. Res. Soc. Bull.* **2004**, *29*, 940–965.
10. Funke, O.; Phanikumar, G.; Galenko, P.K.; Chernova, L.; Reutzel, S.; Kolbe, M.; Herlach, D.M. Dendrite growth velocity in levitated undercooled nickel melts. *J. Cryst. Growth* **2006**, *297*, 211–222.
11. Herlach, D.M.; Matson, D.M. *Solidification of Containerless Undercooled Melts*; Wiley: Weinheim, Germany, 2012.
12. Volkmann, T. Measurements of crystal growth velocities in undercooled melts. In *Solidification of Containerless Undercooled Melts*; Wiley: Weinheim, Germany, 2012.
13. Piller, J.; Knauf, R.; Preu, P.; Herlach, D.M.; Lohöfer, G. Containerless Positioning and inductive heating under micro-g conditions. In Proceedings of the 6th European Symposium on Materials Sciences under Microgravity, Bordeaux, France, 2–5 December 1986.
14. Kurz, W.; Fischer, D.J. *Fundamentals of Solidification*, 3rd ed.; Trans Tech Publications: Aedermannsdorf, Switzerland, 1989.

15. Galenko, P.K.; Sobolev, S. Local non-equilibrium effect on undercooling in rapid solidification of alloys. *Phys. Rev. E* **1997**, *55*, 343–351.
16. Galenko, P.K.; Danilov, D.A. Local non-equilibrium effect on rapid dendrite growth in a binary alloy melt. *Phys. Lett. A* **1997**, *235*, 271–278.
17. Brener, B.; Melnikov, V.J. Pattern selection in two-dimensional dendritic growth. *Adv. Phys.* **1991**, *40*, 53–97.
18. Hoyt, J.J.; Asta, M.; Karma, A. Method for computing the anisotropy of the solid-liquid interfacial free energy. *Phys. Rev. Lett.* **2001**, *86*, 5530–5533.
19. Galenko, P.K. Extended thermo-dynamical analysis of a motion of the solid-liquid interface in a rapidly solidifying alloy. *Phys. Rev. B* **2002**, *65*, doi:10.1103/PhysRevB.65.144103.
20. Galenko, P.K. Solute trapping and diffusion-less solidification in a binary alloy. *Phys. Rev. E* **2007**, *76*, doi:10.1103/PhysRevE.76.031606.
21. Kerrache, A.; Horbach, J.; Binder, K. Molecular-dynamics computer simulation of crystal growth and melting in Al<sub>50</sub>Ni<sub>50</sub>. *Europhys. Lett.* **2008**, *81*, doi:10.1209/0295-5075/81/58001.
22. Alexandrov, D.V.; Galenko, P.K. Selection criterion of stable dendritic growth at arbitrary Péclet numbers with convection. *Phys. Rev. E* **2013**, *87*, doi:10.1103/PhysRevE.87.062403.
23. Herlach, D.M.; Galenko, P.K. Rapid Solidification: In situ diagnostics and theoretical modelling. *Mater. Sci. Eng. A* **2007**, *449–451*, 34–41.
24. Lee, J.; Matson, D.M.; Binder, S.; Kolbe, M.; Herlach, D.M.; Hyers, R.W. Magnetohydrodynamic modeling and experimental validation of convection inside electromagnetically levitated Co-Cu droplets. *Metall. Mater. Trans. B* **2013**, *44*, doi:10.1007/s11663-013-9995-5.
25. Bouissou, P.; Pelce, P. Effect of a forced flow on dendritic growth. *Phys. Rev. A* **1989**, *40*, 6673–6680.
26. Jeong, J.-H.; Goldenfeld, N.; Danzig, J.A. Phase field model for three-dimensional dendritic growth with fluid flow. *Phys. Rev. E* **2001**, *64*, doi:10.1103/PhysRevE.64.041602.
27. Aziz, M.J.; Boettinger, W.J. On the transition from short-range diffusion-limited to collision-limited growth in alloy solidification. *Acta Metall. Mater.* **1994**, *42*, 527–537.
28. Gandham, P.; Biswas, K.; Funke, O.; Holland-Moritz, D.; Herlach, D.M.; Chattopadhyay, K. Solidification of undercooled peritectic Fe–Ge alloy. *Acta Mater.* **2005**, *53*, 3591–3600.
29. Assadi, H.; Reutzel, S.; Herlach, D.M. Kinetics of solidification of B2 intermetallic phase in the Ni–Al system. *Acta Mater.* **2006**, *54*, 2793–2800.
30. Sutton, M.; Yang, Y.S.; Mainville, J.; Jordan-Sweet, J.L.; Ludwig, K.F.; Stephenson, G.B. Observation of a precursor during the crystallization of amorphous NiZr<sub>2</sub>. *Phys. Rev. Lett.* **1989**, *62*, 288–291.
31. Greer, A.L.; Assadi, H. Rapid solidification of intermetallic compounds. *Mater. Sci. Eng. A* **1997**, *226–228*, 133–141.
32. Boettinger, W.J.; Bendersky, L.A.; Cline, J.; West, J.A.; Aziz, M.J. Disorder trapping in Ni<sub>2</sub>TiAl. *Mater. Sci. Eng. A* **1991**, *133*, 592–595.
33. Huang, Y.; Aziz, M.J.; Hutchinson, J.W.; Evans, A.G.; Saha, R.; Nix, W.D. Comparison of mechanical properties of Ni<sub>3</sub>Al thin films in disordered FCC and ordered L1<sub>2</sub> phases. *Acta Mater.* **2001**, *49*, 2853–2861.

34. Boettinger, W.J.; Aziz, M.J. Theory for the trapping of disorder and solute in intermetallic phases by rapid solidification. *Acta Metall.* **1989**, *37*, 3379–3391.
35. Assadi, H.; Greer, A.L. The interfacial undercooling in solidification. *J. Cryst. Growth* **1997**, *172*, 249–258.
36. Boettinger, W.J.; Coriell, S.R.; Greer, A.L.; Karma, A.; Kurz, W.; Rappaz, M.; Trivedi, R. Solidification microstructures: recent developments, future directions. *Acta Mater.* **2000**, *48*, 43–70.
37. Hartmann, H.; Holland-Moritz, D.; Galenko, P.K.; Herlach, D.M. Evidence of the transition from ordered to disordered growth during rapid solidification of an intermetallic phase. *Europhys. Lett.* **2009**, *87*, doi:10.1209/0295-5075/87/40007.
38. Hyers, R.W. Fluid flow effects in levitated droplets. *Meas. Sci. Technol.* **2005**, *16*, 394–401.
39. Reutzler, S.; Hartmann, H.; Galenko, P.K.; Schneider, S.; Herlach, D.M. Change of the kinetics of solidification and microstructure formation induced by convection in the Ni-Al system. *Appl. Phys. Lett.* **2007**, *91*, doi:10.1063/1.2760154.
40. Barth, M.; Wei, B.; Herlach, D.M. Crystal growth in undercooled melts of the intermetallic compounds FeSi and CoSi. *Phys. Rev. B* **1995**, *51*, 3422–3428.
41. Binder, S.; Galenko, P.K.; Herlach, D.M. The effect of fluid flow on the solidification of Ni<sub>2</sub>B from the undercooled melt. *J. Appl. Phys.* **2014**, *115*, doi:10.1063/1.4864151.
42. Binder, S. Faceting of a Rough Solid–Liquid Interface of a Metal Induced by Forced Convection. Ph.D. Thesis, Ruhr-University Bochum, Bochum, Germany, November 2009.
43. Jackson, K.A. On the nature of crystal growth from the melt. *J. Cryst. Growth* **1974**, *24–25*, 130–137.
44. Glicksman, M.E.; Schaefer, R.J. Investigation of solid/liquid interface temperatures via isenthalpic solidification. *J. Cryst. Growth* **1967**, *1*, 297–308.
45. Dantzig, J.A.; Rappaz, M. *Solidification*; EPFL Press: Lausanne, Switzerland, 2009.
46. Porter, D.A.; Easterling, K.E. *Phase Transformations in Metals and Alloys*; Chapman and Hall: London, UK, 1992.
47. Binder, S.; Galenko, P.K.; Herlach, D.M. Faceting of a rough solid–liquid interface of a metal induced by forced convection. *Philos. Mag. Lett.* **2013**, *93*, 608–613.
48. Jackson, K.A.; Uhlmann, D.R.; Hunt, J.D. On the nature of crystal growth from the melt. *J. Cryst. Growth* **1967**, *1*, 1–14.
49. Faure, F.; Trolliard, G.; Nicollet, C.; Montel, J.-M. A development model of olivine morphology as a function of the cooling rate and the degree of undercooling. *Contrib. Mineral. Petrol* **2003**, *145*, 251–260.
50. Garcia-Ruiz, J.M. Growth history of PbS single crystals at room temperature. *J. Cryst. Growth* **1986**, *75*, 441–446.
51. Herlach, D.M.; Galenko, P.K.; Holland-Moritz, D. *Metastable Solids from Undercooled Melts*; Pergamon Materials Series; Cahn, R., Ed.; Pergamon: Oxford, UK, 2007.
52. Greet, R.J.; Magill, J.H. An empirical corresponding-states relationship for liquid viscosity. *J. Phys. Chem.* **1967**, *71*, 1746–1756.
53. Magill, J.H.; Plazek, D.J. Physical properties of aromatic hydrocarbons II: Solidification behavior of 1,3,5-Tri- $\alpha$ -Naphthylbenzene. *J. Chem. Phys.* **1967**, *46*, 3757–3769.

54. Fuss, T.; Ray, C.S.; Lesher, C.E.; Day, D.E. *In situ* crystallization of lithium disilicate glass: Effect of pressure on crystal growth rate. *J. Non Cryst. Solids* **2006**, *352*, 2073–2081.
55. Fokin, V.M.; Nascimento, M.L.F.; Zanotto, E.D. Correlation between maximum crystal growth rate and glass transition temperature of silicate glasses. *J. Non Cryst. Solids* **2005**, *351*, 789–794.
56. Wang, Q.; Wang, L.-M.; Ma, M.Z.; Binder, S.; Volkmann, T.; Herlach, D.M.; Wang, J.; Xue, Q.G.; Tian, Y.J.; Liu, R.P. Diffusion-controlled crystal growth in deeply undercooled Zr<sub>50</sub>Cu<sub>50</sub> melt on approaching the glass transition. *Phys. Rev. B* **2011**, *83*, doi:10.1103/PhysRevB.83.014202.
57. Wang, W.H.; Lewandowski, J.J.; Greer, A.L. Understanding the glass-forming ability of Cu<sub>50</sub>Zr<sub>50</sub> alloys in terms of metastable eutectic. *J. Mater. Res.* **2005**, *20*, 2307–2313.
58. Turnbull, D. Under what conditions can a glass be formed? *Contemp. Phys.* **1969**, *10*, 473–488.
59. Oh, S.H.; Kauffmann, Y.; Scheu, C.; Kaplan, W.D.; Rühle, M. Ordered liquid aluminum at the interface with sapphire. *Science* **2005**, *310*, 661–663.
60. Oh, S.H.; Chisholm, M.F.; Kauffmann, Y.; Kaplan, W.D.; Luo, W.; Rühle, M.; Scheu, C. Oscillatory mass transport in vapor-liquid-solid growth of sapphire nanowires. *Science* **2010**, *330*, 489–493.
61. Jackson, K.A. The interface kinetics of crystal growth processes. *Interface Sci.* **2002**, *10*, 159–169.
62. Ediger, M.D.; Harrowell, P.; Yu, L. Crystal growth kinetics exhibit a fragility-dependent decoupling from viscosity. *J. Chem. Phys.* **2008**, *128*, doi:10.1063/1.2815325.
63. Hoyt, J.J.; Asta, M. Atomistic computation of liquid diffusivity, solid-liquid interfacial energy, and kinetic coefficient in Au and Ag. *Phys. Rev. B* **2002**, *65*, doi:10.1103/PhysRevB.65.214106.
64. Ashkenazy, Y.; Averbach, R.S. Kinetic stages in the crystallization of deeply undercooled body-centered-cubic and face-centered-cubic metals. *Acta Mater.* **2010**, *58*, 524–530.
65. Tang, C.G.; Harrowell, P. Anomalously slow crystal growth of the glass-forming alloy CuZr. *Nat. Mater.* **2013**, *12*, 507–511.
66. Brillo, J.; Pommrich, A.I.; Meyer, A. Relation between self-diffusion and viscosity in dense liquids: new experimental results from electrostatic levitation. *Phys. Rev. Lett.* **2011**, *107*, doi:10.1103/PhysRevLett.107.165902.
67. Holland-Moritz, D.; Stüber, S.; Hartmann, H.; Unruh, T.; Meyer, A. Ni-self diffusion in Zr-Ni(-Al) melts. *J. Phys. Conf. Ser.* **2009**, *144*, 012119.
68. Bragard, J.; Karma, A.; Lee, Y.H.; Plapp, M. Linking phase-field and atomistic simulations to model dendritic solidification in highly undercooled melts. *Interface Sci.* **2002**, *10*, 121–136.
69. Meyer, A.; Wuttke, J.; Petry, W.; Randl, O.G.; Schober, H. Slow motion in a metallic liquid. *Phys. Rev. Lett.* **1998**, *80*, 4455–4457.
70. Faupel, F.; Frank, W.; Macht, M.P.; Mehrer, H.; Naundorf, V.; Rätzke, K.; Schober, R.; Sharma, S.K.; Teichler, H. Diffusion in metallic glasses and supercooled melts. *Rev. Mod. Phys.* **2003**, *75*, 237–280.